

AIP | Review of Scientific Instruments

Tunable optical tweezers for wavelength-dependent measurements

Brooke Hester, Gretchen K. Campbell, Carlos López-Mariscal, Carly Levin Filgueira, Ryan Huschka et al.

Citation: *Rev. Sci. Instrum.* **83**, 043114 (2012); doi: 10.1063/1.4704373

View online: <http://dx.doi.org/10.1063/1.4704373>

View Table of Contents: <http://rsi.aip.org/resource/1/RSINAK/v83/i4>

Published by the [American Institute of Physics](http://www.aip.org).

Related Articles

Light-driven three-dimensional rotational motion of dandelion-shaped microparticles

Appl. Phys. Lett. **102**, 071103 (2013)

Analysis of optical and electrical crosstalk in small pitch photon trapping HgCdTe pixel arrays

Appl. Phys. Lett. **101**, 261118 (2012)

Thin-film silicon triple-junction solar cell with 12.5% stable efficiency on innovative flat light-scattering substrate

J. Appl. Phys. **112**, 114503 (2012)

Guided-mode quantum efficiency: A novel optoelectronic characterization technique

Rev. Sci. Instrum. **83**, 114704 (2012)

Light trapping in solar cells: When does a Lambertian scatterer scatter Lambertianly?

J. Appl. Phys. **112**, 094504 (2012)

Additional information on *Rev. Sci. Instrum.*

Journal Homepage: <http://rsi.aip.org>

Journal Information: http://rsi.aip.org/about/about_the_journal


Top downloads: http://rsi.aip.org/features/most_downloaded

Information for Authors: <http://rsi.aip.org/authors>

ADVERTISEMENT

JANIS

Does your research require low temperatures? Contact Janis today.
Our engineers will assist you in choosing the best system for your application.



- 10 mK to 800 K
- LHe/LN₂ Cryostats
- Cryocoolers
- Magnet Systems
- Dilution Refrigerator Systems
- Micro-manipulated Probe Stations

sales@janis.com www.janis.com
Click to view our product web page.

Tunable optical tweezers for wavelength-dependent measurements

Brooke Hester,^{1,a)} Gretchen K. Campbell,² Carlos López-Mariscal,^{3,b)}
Carly Levin Filgueira,⁴ Ryan Huschka,⁴ Naomi J. Halas,⁵ and Kristian Helmerson^{6,b)}

¹*Physics and Astronomy Department, Appalachian State University, 525 Rivers Street, Boone, North Carolina 28608, USA*

²*National Institute of Standards and Technology, Gaithersburg, Maryland 20814, USA*

³*US Naval Research Laboratory, Washington, DC 20375, USA*

⁴*Department of Chemistry, Rice University, Houston, Texas 77251-1892, USA*

⁵*Departments of Chemistry, Biomedical Engineering, Physics and Astronomy, and Electrical and Computer Engineering, Rice University, Houston, Texas 77251-1892, USA*

⁶*School of Physics, Monash University, Clayton, Victoria 3168, Australia*

(Received 17 November 2011; accepted 2 April 2012; published online 23 April 2012)

Optical trapping forces depend on the difference between the trap wavelength and the extinction resonances of trapped particles. This leads to a wavelength-dependent trapping force, which should allow for the optimization of optical tweezers systems, simply by choosing the best trapping wavelength for a given application. Here we present an optical tweezer system with wavelength tunability, for the study of resonance effects. With this system, the optical trap stiffness is measured for single trapped particles that exhibit either single or multiple extinction resonances. We include discussions of wavelength-dependent effects, such as changes in temperature, and how to measure them. [<http://dx.doi.org/10.1063/1.4704373>]

I. INTRODUCTION

Optical tweezers have been shown to be a flexible and useful tool for the manipulation of small objects from the nanometer scale to the micrometer scale.^{1,2} A conventional optical tweezer system consists of a highly focused laser beam, some basic optics, and detection electronics. Optical tweezers have been used to study biological systems including those at the single molecule level,³ properties of fluids,⁴ systems of colloids,⁵ and are also used as tools for manipulation techniques for high resolution position sensing.⁶ While many experiments have examined the physics of the trapping forces in optical tweezers systems, effects of the trapping wavelength on optical forces and the optical properties of the trapped particle have not been previously analyzed. Here, we describe the design, construction, and implementation of a new optical tweezer apparatus, and show how it can be used to investigate wavelength-dependent effects. In particular, we investigate the effect of wavelength on trap stiffness, and study the interplay between trapping wavelength and optical properties.

The trapping laser wavelength should play a strong role in optimizing the optical forces of a tweezer system. Therefore, our new apparatus can be used for determining the optimal trapping wavelengths for a number of applications such as optical sorting^{7,8} and binding,⁹ low-optical-power tweezing, and the prevention of thermal damage to delicate biological systems,¹⁰ and the selective exertion of strong forces on small objects in a crowded environment.¹¹ In addition, our home-

built apparatus is more cost-efficient than those based on commercial microscopes. While it is true that optical tweezers are typically able to trap a particle regardless of its resonance, experimentalists generally lack the ability to determine the optimal trapping wavelength. This is important for applications where minimal heating¹² or maximal forces¹³ are desired.

Properties of nano- and micron-scale objects, such as the complex refractive index, depend on wavelength. Our apparatus will be useful for optical wavelength-dependent measurements of single micro- and nano-particles. The bulk properties of a material can differ greatly from those at the nanoscale.¹⁴ This optical system will provide a means for the measurement of those smaller-scale properties for single particles surrounded by a uniform fluid, preventing the need for a substrate.^{15–17}

Although optical forces due to a near-resonant laser beam have been studied extensively for atoms, the situation for larger particles has only been studied numerically.¹⁸ A Rayleigh particle, one that is much smaller than the wavelength of the light incident upon it, is expected to behave much like an atom in an optical trap.¹⁹ The small size of the particle compared to the large uniform electric field results in a dipole response. In such a case, the optical forces are dominated by the complex polarizability of the particle, which is inherently linked to the extinction (scattering plus absorption) resonance of the particle. The total trapping force is a sum of the gradient and scattering forces. The gradient force arises from the strong intensity gradient of the highly focused laser beam and the scattering force is due to the radiation pressure. The gradient force which is mostly responsible for trapping increases as the trapping wavelength approaches the resonance from the red side (i.e., the longer wavelength side), comes to a maximum close to the absorption resonance wavelength, and drops sharply at the scattering resonance. On the blue (shorter wavelength) side of the absorption

^{a)}Formerly at Chemical Physics Program, University of Maryland, College Park, Maryland 20742, USA and National Institute of Standards and Technology, Gaithersburg, Maryland 20814, USA. Electronic mail: hesterbc@appstate.edu.

^{b)}Formerly at: National Institute of Standards and Technology, Gaithersburg, Maryland 20814, USA.

resonance, the gradient force is repulsive and so no trapping is expected.¹⁹ For larger particles whose size is on the order of a wavelength, predictions of the trapping force require rigorous numerical calculations and cannot be viewed with such a simple picture. In this regime, wavelength-dependent Mie scattering resonances can occur. For some trapping schemes with polystyrene particles, this wavelength dependence has been considered, and maximal trapping forces were determined to exist when the ratio of particle radius to trap wavelength is on the order of one half to three-quarters.¹⁸ We expect enhanced optical forces near a resonance for Rayleigh particles and for particles whose size is comparable to the trap wavelength. Previously, optical forces and their relationship to optical resonances have been studied in an optical levitation scheme over short laser wavelength ranges²⁰ and for dye-loaded dielectric particles.²¹ In the first case, since the particles were not actually optically trapped, only the scattering force and not the gradient force was considered. In the second case, the trap strength measurements were normalized by beads lacking dye, meaning that only the absorption resonance, and not the total extinction resonance, was considered. By considering the total extinction resonance of a trapped particle over an optimized trapping wavelength range, this should allow for a significant increase in trapping forces. We present here a new optical tweezers system designed for measurements that are wavelength dependent and for experiments that require measurements at several wavelengths.

II. MATERIALS AND METHODS

A. Experimental apparatus

The apparatus is based on a custom-built horizontal microscope (Fig. 1). Optical components⁴¹ are from Thorlabs, Newport, COMAR, New Focus, and Edmund Optics, and are mounted on two separate optical tables designed for vibration reduction. The beam paths remain parallel to the optical tables and their heights are minimized to reduce drift and vibration. For the trapping and detection lasers, we can use either a CW TEM_{00} linearly polarized Titanium:sapphire (Ti:sapphire) laser (900 mW at 790 nm, Del Mar Photonics, San Diego, CA), tunable from 730 nm to 860 nm using a birefringent crystal filter, or a CW linearly polarized diode pumped Nd:YAG laser (1064 nm, 1.5 W, OEM laser systems, East Lansing, Michigan). The system is designed such that these lasers can be used independently or concurrently. The lasers are aligned into the microscope so that their beam focuses overlap and particles may be exchanged from one trap to the other and measured in either trap. To maximize pointing stability, the Ti:sapphire laser is fiber coupled from a second optical table. Reflections which cause mode-hopping and instabilities are prevented from entering the Ti:sapphire with an optical beam isolator (BI) (IO-3-800-HP, OFR, Newton, NJ). The wavelength of the Ti:sapphire beam is continuously measured with a fiber spectrometer (USB2000, Ocean Optics, Dunedin, FL). The polarization of the linearly polarized beam is controlled with a half-wave plate (W1) and a polarizing beamsplitter cube (PBS1) to ensure optimized coupling into the polarization-maintaining optical fiber (PMF). A focusing lens (FL) is used to couple the beam into the PMF (OZ optics, Ottawa, Ontario, Canada) which transfers the beam between breadboards (PBH1112, Thorlabs, Newton, NJ) (63-530, TMC, Peabody, MA). A collimating lens (CL) (OZ optics, Ottawa, Ontario, CA) is used on the output of the fiber to create a beam with a diameter of 4 mm. A beam sampler (BS) (BSP 10-B1, Thorlabs, Newton, NJ) reflects 4% of the incident light to a photodiode (PD) (SM1PD1A, Thorlabs, Newton, NJ). The signal of the photodiode is amplified using a low noise current preamplifier (SR570, SRS, Sunnysvale, CA), and monitored with an oscilloscope (TDS2014, Tektronix, Beaverton, OR) for optical power tracking. Lenses (L1 and L2) form a telescope and increase the beam diameter by a factor of 1.8 in order to optimally overfill the back aperture of the trapping microscope objective lens. These lenses are placed so that the back-focal-plane of the trapping objective lens (MO1) is imaged onto the steering mirror M1.

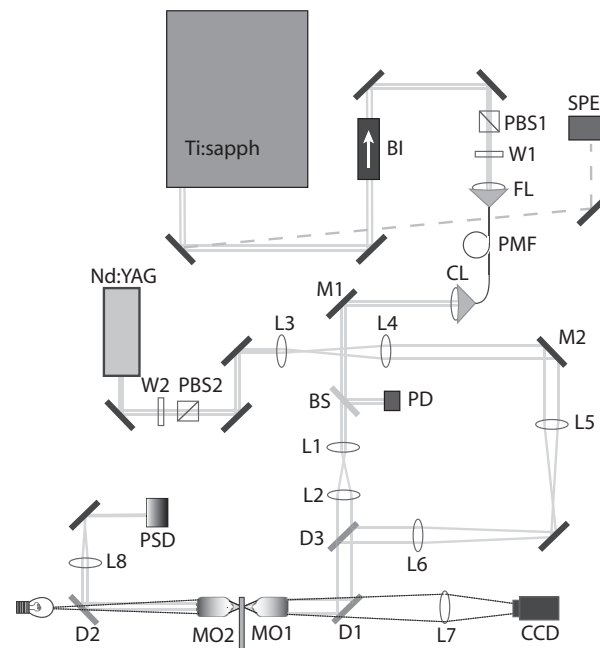


FIG. 1. Experimental optical tweezers setup for wavelength-dependent measurements.⁴¹ The Ti:sapphire laser is isolated from back reflections with an optical isolator (BI). The polarization of the Ti:sapphire beam, which serves as the wavelength-tunable source for the optical tweezers, is adjusted with a waveplate (W1) and polarizing beamsplitter (PBS1) and sent through a polarization-maintaining optical fiber. A focusing lens (FL) couples the beam into the fiber and a collimating lens (CL) collimates the beam. A spectrometer (SPEC) is used to monitor the laser beam wavelength. The optical power of the Ti:sapphire beam is monitored using a beam sampler (BS) and photodiode (PD). Two lenses (L1 and L2) serve as a telescope for increasing the Ti:sapphire beam diameter and are placed such that the mirror (M1) can be used as a steering mirror. A dichroic mirror (D1) reflects the Ti:sapphire beam into the microscope objective (MO1) used both to create the optical trap and as the imaging lens in our microscope. Another microscope objective (MO2) collects the light and serves as the condensing lens for our microscope. A second dichroic mirror (D2) reflects the Ti:sapphire beam to the position-sensing detector (PSD). A lens (L8) is used to project the back focal plane of MO2 onto the PSD. The power of a second laser, Nd:YAG, is adjusted with a waveplate (W2) and polarizing beamsplitter (PBS2) and a telescope (L3 and L4) is used to increase the Nd:YAG beam diameter and to allow M2 to be the Nd:YAG beam steering mirror. The Nd:YAG beam is coupled onto the same path as the Ti:sapphire beam with a dichroic mirror (D3). A lamp and charge coupled device (CCD) camera are used for viewing the trapping plane.

lens (FL) is used to couple the beam into the PMF (OZ optics, Ottawa, Ontario, Canada) which transfers the beam between breadboards (PBH1112, Thorlabs, Newton, NJ) (63-530, TMC, Peabody, MA). A collimating lens (CL) (OZ optics, Ottawa, Ontario, CA) is used on the output of the fiber to create a beam with a diameter of 4 mm. A beam sampler (BS) (BSP 10-B1, Thorlabs, Newton, NJ) reflects 4% of the incident light to a photodiode (PD) (SM1PD1A, Thorlabs, Newton, NJ). The signal of the photodiode is amplified using a low noise current preamplifier (SR570, SRS, Sunnysvale, CA), and monitored with an oscilloscope (TDS2014, Tektronix, Beaverton, OR) for optical power tracking. Lenses (L1 and L2) form a telescope and increase the beam diameter by a factor of 1.8 in order to optimally overfill the back aperture of the trapping microscope objective lens. These lenses are placed so that the back-focal-plane of the trapping objective lens (MO1) is imaged onto the steering mirror M1.

A dichroic mirror (D1) (XF2033, Omega Optical, Brattleboro, VT) reflects the Ti:sapphire beam into an oil-immersion trapping microscope objective lens (MO1) (63X, 1.4 NA, Plan Apochromat oil, 440760, Zeiss, Thornwood, NY) and transmits visible light for imaging. Another microscope objective lens (MO2) (40X, 0.6NA, 440864, LD Achromplan air, Zeiss, Thornwood, NY) collects the forward-scattered light. A Helium:Neon laser (not shown) is used to align the two microscope objectives so that they are aligned along the central axis of the microscope. After MO2, the Ti:sapphire beam is reflected from a dichroic mirror (D2) (XF2033, Omega Optical, Brattleboro, VT) and a lens (L7) is placed so that the back focal plane of MO2 is projected onto a duolateral position sensing detector (PSD) (210LSP, On-Trak Photonics, Inc., Lake Forest, CA). Resulting voltage signals are amplified with a voltage amplifier (OT301, On-Trak, Irvine, CA) and measured with a data acquisition card (PCI-6221, National Instruments, Austin, TX) controlled by custom-made LABVIEW programs.

The power of the Nd:YAG laser is controlled with a half-waveplate (W2) and a polarizing beamsplitter cube (PBS2). Lenses L3 and L4 form a 1:3 telescope and increase the beam diameter in order to optimally overfill the back aperture of MO1. Lenses L5 and L6 form a 1:1 telescope and are placed such that the mirror M2 is a steering mirror for the Nd:YAG beam. M2 is mounted on a piezo-actuated mirror mount (AG-M100N, Newport, Irvine, CA) for high resolution beam steering. A dichroic mirror (D3) (XF2016, Omega Optical, Brattleboro, VT) combines the Nd:YAG beam with the Ti:sapphire beam path. The Nd:YAG beam follows the same path as the Ti:sapphire beam after the dichroic. A microscope lamp illuminates the sample placed between the microscope objective lenses and a lens (L7) acts as an imaging lens for projecting the trapping plane onto a charge coupled device (CCD) camera.

The sample chamber is formed with two microscope coverslips (22x22-0, Fisherbrand, Waltham, MA) separated by a 0.5 mm silicone spacer (JTR-S-0.5, Grace BioLabs, Bend, OR) and sealed with silicone vacuum grease (Dow Corning, Midland, MI). The chamber is placed on a custom-built mount which slides easily between the microscope objectives and remains aligned to a plane normal to the direction of light propagation. The mount is fixed to a three-axis stage whose motion can be controlled by three high-resolution (20 nm step size) Picomotors (New Focus, Santa Clara, CA). Before each experiment, the sample chamber is filled with purified and deionized water and a small amount of particles. The concentration of particles is chosen such that only one particle will diffuse into the trap every ten minutes. A conventional commercial inverted microscope could have been used for this experiment, but for our purposes, a custom-built system was more versatile and allowed for us to easily make changes as the apparatus evolved.

Using this apparatus, we have trapped gold nanoshells in addition to polystyrene and silica microspheres. A gold nanoshell is a small silica sphere coated with a thin, uniform layer of gold.²² Based on the overall size and the gold thickness, the nanoshell extinction resonance can be tuned from the visible to the infrared. We have trapped a range

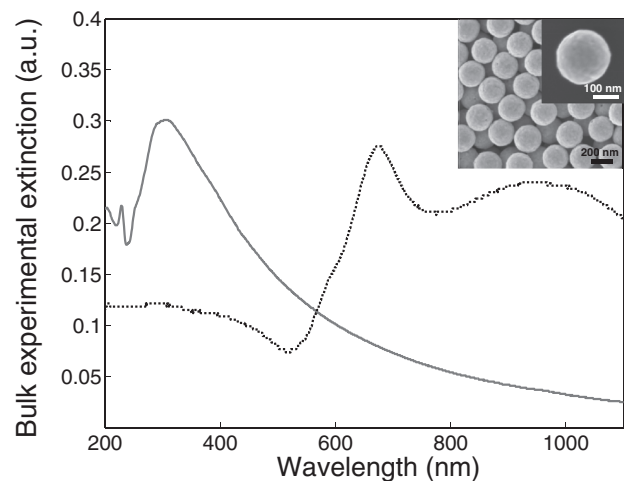


FIG. 2. Experimental extinction spectra of gold nanoshells in bulk (black dotted line) and polystyrene spheres in bulk (grey solid line) used in this study. The polystyrene spheres have a radius of $0.295 \mu\text{m}$. Two peaks are evident in the gold nanoshell spectrum. The one at 680 nm is the absorption peak and the one centered at 980 nm is the scattering peak. The silica core of each nanoshell has a radius of 90 nm while the gold coating is 18 nm thick. For gold nanoshells, these peaks grow further apart as the overall size of the particle increases.²² Inset: SEM image of gold nanoshells.

of nanoshells with diameters ranging from 100 nm to 200 nm , with extinction resonances centered at wavelengths from 650 nm to 1100 nm . Gold nanoshells serve as the Rayleigh particles for this experiment. We have also optically trapped uncoated polystyrene and silica spheres ranging in diameter from 100 nm to $5.5 \mu\text{m}$ (Bangs Laboratories, Fishers, IN). Figure 2 shows the bulk experimental extinction spectra for the two species presented in detail in this work. The spectra are measured with a Spectronic Genesys 5 spectrophotometer (Thermo Fisher, Waltham, MA). Both measurements are performed for bulk particles in water. The extinction resonance peak for the gold nanoshells is at 980 nm . The radius of the silica in the gold nanoshell is 90 nm and the overall radius is 108 nm , giving a gold shell with a thickness of 18 nm . The extinction resonance peak for the polystyrene spheres is at 306 nm and the radius of these particles is $0.295 \mu\text{m}$. These measured spectra are for bulk particles in water and typically will exhibit peak broadening due to particle-to-particle inhomogeneities, as compared to a spectrum for a single particle. However, the feature of interest, the wavelength corresponding to the extinction maximum, is not affected unless those inhomogeneities are extreme and abundant. As shown in the inset in Fig. 2, the gold nanoshells utilized in this study are quite uniform in size and shape.

B. Wavelength calibration techniques

In an optical tweezer, a stable trapped particle is confined to an effective harmonic potential and can be described as an overdamped oscillator subject to the Langevin force arising from thermal fluctuations.²³ The power spectral density of the displacement of the particle is Lorentzian in shape²⁴ and has

the form

$$S_x(f) = \frac{k_B T}{2\pi^2 \beta (f_0^2 + f^2)}, \quad (1)$$

where k_B is Boltzmann's constant, T is temperature, and $\beta = 6\pi\eta r$ is the drag coefficient determined by Stokes' law, where η is the fluid viscosity, and r is the particle radius. The viscosity of water, the background medium in this experiment, is temperature dependent, as described by Laliberté for temperature in Celsius.²⁵

$$\eta(T) = \frac{T + 246}{(0.05594T + 5.2842)T + 137.37}. \quad (2)$$

The corner frequency or roll-off frequency $f_0 = \kappa(2\pi\beta)^{-1}$ is proportional to the trap stiffness, κ , and provides for a measurement of κ .²⁶ In our apparatus, the motion of the trapped particle is tracked using a back focal plane detection technique.²⁷ Intensity shifts arising from the interference of unscattered and scattered laser light occur in the back focal plane of the collecting microscope objective and are recorded with a position sensitive detector. This allows for a measurement of the position of the particle as a function of time. We record the motion of the trapped particle for fifteen to twenty seconds at an acquisition rate of 15 kHz. We then fit a Lorentzian to the power spectrum and determine the corner frequency as shown in Figure 3. This is repeated for the same particle at several trapping wavelengths. Following the method of Neuman and Block,²⁸ we obtained the conversion factor between voltage and displacement by monitoring the displacement voltage of a sphere of known radius stuck to the coverslip surface as the coverslip was translated using the picomotor-driven stage. This technique allows for displacement to be displayed on the vertical axis. In order to use the corner frequency to find the trap stiffness, κ , the drag coefficient β must also be determined. The drag

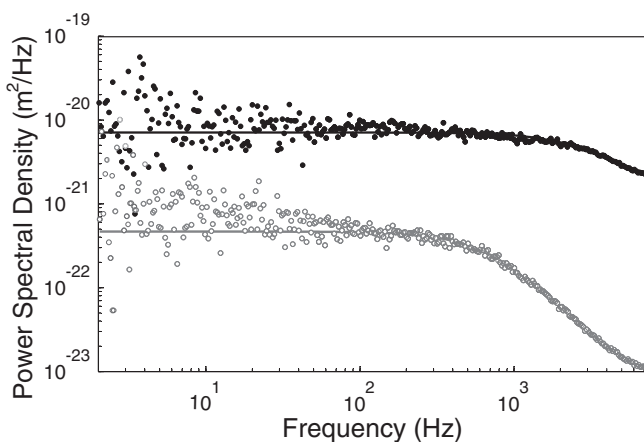


FIG. 3. Power spectra of the trapped nanoshell and polystyrene sphere described in Figure 2. The trapping wavelength was 760 nm. The nanoshell (black dots) was trapped with 54 mW and the polystyrene sphere was trapped with 40 mW (grey circles). The black (nanoshell) and grey (sphere) lines show Lorentzian fits for each experimental data set. The size of the data points reflects the error in the measurement. The laser power was monitored via a pickoff and photodiode and the system was calibrated such that the optical power listed here is an upper-bound for the optical power at the sample plane. This calibration technique is described at the end of the wavelength calibration techniques section.

coefficient depends on both the particle size and the surrounding fluid viscosity. The trap stiffness depends on many factors including the optical power, the diameter of the beam entering the back aperture of the objective lens, the refractive index of the particle and surrounding medium, and the distance of the trapped particle from the surface. In order to highlight the wavelength-dependent changes in trap stiffness, changes in these other factors are minimized for trapped particles over the entire wavelength range. However, the fluid viscosity changes dramatically with temperature, and therefore must be determined for each data point. For each individual gold nanoshell or dielectric sphere, the particle is trapped with light starting at one end of the tunable trapping wavelength spectrum. We then record the motion of a single particle as a function of wavelength, and ensure that the experimental parameters across the wavelength range are constant.

As previously mentioned, only one particle is trapped at a time. Although the polystyrene spheres are easily imaged, the nanoparticles are not visible in the light microscope, so a different method is required for ensuring that only one particle is in the optical trap. If a second particle or multiple particles enter the trap, the voltage signals on the PSD change significantly. If a histogram is made of the position data, the histogram is Gaussian, but the histogram widens and the peak height decreases if more than one particle is trapped.²⁹ In addition, the power spectrum corner frequency also increases when two metallic nanoparticles are trapped and the standard deviation of the voltage signal increases step-wise in amplitude with trapped particle number.³⁰ We performed several measurements for nanoshells and found a minimum voltage signal variance, standard deviation, and corner frequency which correspond to single gold nanoshells. During data analysis, we compare these characteristic signals to the data in question to ensure that only one particle was trapped for each data set. Images of larger particles (0.3 μm and higher) are visible in the light microscope and therefore multiple particle trapping is simple to detect. The effect of multiple-trapped spheres on the PSD voltage is also quite pronounced for larger spheres. Voltage signal variances increase by a factor of about two, and the corner frequency of the power spectrum will generally reduce by half when trapping two large dielectric particles as compared to one.³¹

In order to measure the trap stiffness of a particle with both lasers, a complete overlap of the focus of the two trapping beams was necessary. This was achieved by first trapping a sphere with one laser and recording an image with the CCD camera. Then an identical sphere was trapped with the second laser. The steering mirror for the trap from the second laser was moved so that the trapped sphere overlapped perfectly with the image of the trapped sphere from the first laser. This process was repeated with smaller and smaller spheres until the traps were aligned. In order to collect data for one particle with both traps, the particle was first trapped with the Nd:YAG laser and data was collected. The optical power of the Ti:sapphire laser was slowly ramped up until it reached a maximum. The optical power of the second laser was then slowly decreased. The particle remained in the trapping volume throughout this process if sufficient alignment

was achieved. The optical power of the Ti:sapphire laser was then adjusted for taking data.

The apparatus was constructed to measure the effect of wavelength on the trapping of nanoshells and dielectric spheres. Therefore, we attempted to minimize all other wavelength-dependent trap changes. In order to minimize chromatic aberration, all lenses were achromats. Changing the wavelength from one end of the Ti:sapphire spectrum to the other did not affect the fiber coupling efficiency. Still, we felt it was important to determine the effects of chromatic aberration over the wavelength range. The beam diameter was measured at the entrance to the trapping objective lens and at a second location 20 cm further “downstream” with the dichroic mirror D1 removed. In both cases, the beam diameter increased in size by 5% from 730 nm to 860 nm. We also calculated and measured the beam waist size at the focus after the objective lens. Changes in the beam waist were measured by moving the sample stage in the axial direction such that the beam focus occurred at the inner face of the coverslip. The reflection of the focused beam was imaged on the CCD camera. The pixel size of the collected image was calibrated using a 100 LP/mm Ronchi ruling (NT38-562, Edmund Optics, Barrington, NJ). Images were collected at each trapping wavelength and compared in order to determine changes in the beam waist size. With this technique, the $1/e^2$ measured beam waist size for 730 nm trap light was 824 nm and for 850 nm light was 720 nm, for a difference of 12%. Although this measurement technique gives the beam waist when the beam is focused on the coverslip and not at the actual trapping plane, we expect that the changes in the beam waist over the wavelength range will not differ greatly at the two axial focus positions. Calculations of the beam waist were performed with PSF Lab,³² and took into account microscope objective design characteristics, true experimental parameters which differed from those in the design (i.e., the coverslip thickness used for the experiment and input into PSF Lab was 0.15 mm but the trapping microscope objective was designed for 0.17 mm coverslips), and other details particular to our experiment. The calculated beam waist for 850 nm light was 784 nm and for 730 nm light was 861 nm, for a difference of 8.9%. The $\approx 10\%$ difference in beam waist size should affect the optical trapping forces somewhat. Curiously, for both the measured and calculated values, the beam waist decreases in size with an increase in wavelength. This trend opposes that predicted by a general knowledge of diffraction. In general, the beam should focus more tightly for smaller wavelengths. This does occur when the beam waist size is calculated with PSF Lab over a larger range (from 300 nm to 900 nm). For this particular system, the effects of the nonideal parameters such as mismatched indices of refraction and coverslip thickness contribute to unexpected light focusing in the 730 nm to 860 nm laser wavelength range. The dependence of trap stiffness on changes in beam waist size will therefore be highly dependent on the details of a particular system, and would need to be tested with particles that are known to have no resonance near or within the experimental wavelength range.

In order to further test the wavelength-dependent focusing effects of the trapping microscope objective, the axial shift of the focus was also measured. First, the picomotor control-

ling the stage in the axial direction was calibrated. This was achieved by trapping a polystyrene sphere and then by slowly moving the stage a noted number of steps towards the edge of the sphere. The spheres used for this particular measurement stuck very easily to the coverslip, so once the sphere came into contact with the glass surface, motion would immediately stop and become unaffected by the laser trap. The position signal and the power spectrum of the sphere were observed in real time. Based on Faxen’s law and the fact that the trap stiffness is dependent on Stokes’ drag,²⁶ the position signal and the power spectrum signal are sensitive to changes in distance between the trapped particle and the chamber surface. When the signals suddenly matched those of a stuck sphere, it was determined that the coverslip was touching the edge of the sphere. The sphere was then released from the trap by temporarily blocking the beam, and the picomotor was moved a noted number of steps until the reflection from the coverslip was minimized in diameter, meaning the coverslip was located at the beam focus. The radius of the sphere was known, and the distance from the beam focus to the center of the trapped sphere was determined based on Neuman and Block.²⁸ The distance traveled by the coverslip should equal the displacement of the center of the sphere from the beam focus subtracted from the radius of the sphere. In this manner, the step size of the picomotor was calibrated and determined to be 8 ± 1 nm when the picomotor moved the sample chamber away from the microscope objective at a frequency of 100 Hz. With this picomotor step size calibration, the axial beam focus shift was measured as a function of wavelength. Using the Ti:sapphire laser, the CCD camera recorded an image of the back reflection of the trap light from the coverslip at 860 nm. The trap light was then scanned to the other end of the spectrum at 730 nm while maintaining a constant optical power incident upon the CCD camera. The axial direction picomotor was then used to move the coverslip until the diameter of the back reflection of the trap at 730 nm was the same as that measured at 860 nm. The number of steps was noted, and the distance traveled was calculated to be $400 \text{ nm} \pm 100 \text{ nm}$, meaning that over the entire wavelength range, the beam focus shifts 400 nm further away from or closer to the edge of the sample chamber. This could affect trap stiffness in two ways. First, spherical aberrations in the Gaussian profile of the trapping laser beam can increase or decrease with changes in distance from the coverslip to the beam focus, as a function of the index of refraction of the immersion liquid, of the coverslip glass, and of the fluid inside the sample chamber.³³ Second, for a particle whose radius is comparable to the quantity ξ , the distance from a particle’s center to the coverglass surface, large changes in the viscous drag can occur. We avoid this complication by keeping ξ at least four times the sphere radius. In order to test the effects of spherical aberration from changes in ξ , we trapped single particles and measured the corner frequency at several values of ξ . For a single trapped nanoshell, the corner frequency typically decreases by a factor of two when ξ increases by $10 \mu\text{m}$. For a single trapped polystyrene sphere ($0.94 \mu\text{m}$ in diameter) the corner frequency increases by a factor of 1.6 with an increase in ξ by $9 \mu\text{m}$. How spherical aberrations affect the trapping forces is highly dependent on both particle size and ξ , hence

the discrepancy in trends for the two particles. At any rate, for a small change in ξ , small changes in corner frequencies are expected. Based on the measurements described here, the change in ξ (400 nm) due to the maximum change in wavelength should not contribute to more than a 10% increase or decrease in the corner frequency.

Another possible effect caused by changing the wavelength is the performance of the Ti:sapphire laser. As the Ti:sapphire wavelength is varied, starting from 730 nm, the maximum power slowly increases and reaches a maximum at 790 nm, and as the wavelength is increased further, the power decreases again to a minimum at 860 nm. As discussed, it is important to keep all parameters constant while changing wavelength, and so a scheme was developed to ensure constant laser power. The photodiode (PD) in Figure 1 measures changes in the optical power from a pickoff reflection of the Ti:sapphire laser beam. The photodiode current is converted to voltage and recorded simultaneously with the voltage signals from the PSD during data collection, allowing for a measure of trap power at any given time. A calibration was also carried out to ensure that the PD voltage gives an accurate measurement of the optical power at the trapping plane. Since the corner frequency of a trapped particle increases linearly with the trap optical power, we simultaneously measured the PD voltage and the corner frequency for a large (4.84 μm) polystyrene sphere. For a particle of this size the optical resonances should not affect the stiffness over the wavelength range. Not surprisingly, the measured corner frequency and the measured voltage coincide in shape across the trapping wavelength range as the maximum trap power changes, as shown in Figure 4, left inset. The change in the corner frequency follows the same basic path as the change in measured voltage, or essentially the change in optical power. It should follow that a constant voltage at the PD should result in a constant optical power level at the trapping plane regardless of the trapping wavelength. In order to verify this assumption, the optical power at the trapping plane was measured directly with an optical power meter (FieldMate,

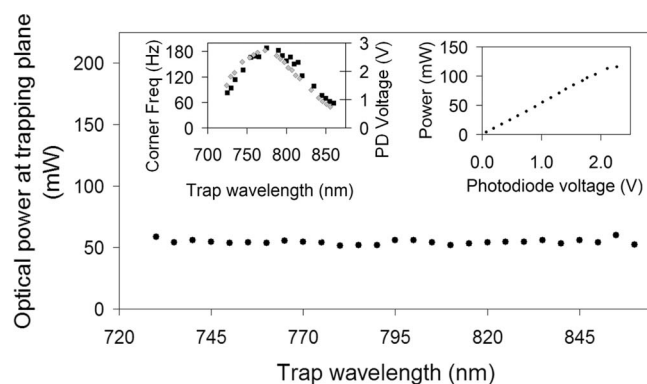


FIG. 4. Measured optical power after the trapping microscope objective for constant voltage on the power-monitor photodiode. Inset left - Measured corner frequency for a polystyrene sphere trapped over the wavelength range with maximum power at each wavelength. Black squares are the measured corner frequency of the trapped particle and grey diamonds are the measured voltages from the power tracking photodiode (PD). Inset right - Optical power vs. photodiode voltage calibration curve: The measured power after the trapping microscope objective as a function of photodiode voltage.

Coherent, Santa Clara, CA) while monitoring the PD voltage. The laser power was controlled by adjusting the power of the pump laser for the Ti:sapphire at each wavelength, such that the PD voltage remained constant. Light exiting the trapping microscope objective (MO1) was collimated onto the power meter detector by removing L1 from the beam path only for this measurement. This results in L2 and MO1 becoming a telescope pair, since L2 was already placed at a distance equal to its focal length away from MO1, so collimated light entering L2 should also be collimated when it exits MO1. As expected the measured optical power after MO1 remained essentially constant for a given photodiode voltage as the wavelength was varied (Figure 4). While the photodiode response increased slightly over the wavelength range, the microscope objective transmission decreased comparably over the wavelength range, resulting in this constant photodiode reading corresponding to a constant optical power at the sample plane. A calibration curve was generated for the optical power of the trap as a function of measured photodiode voltage (Figure 4, right inset). In order to control the optical power at the sample plane in practice, the optical power of the Ti:sapphire laser was adjusted manually by controlling the optical power of its pump laser until the desired photodiode voltage was achieved, using the calibration curve in Figure 4 (right inset). This was repeated for each wavelength used.

C. Temperature and viscosity effects

Trap stiffness, κ , determined from the corner frequency measurement, depends linearly on the viscosity, η , of the fluid surrounding the trapped particle, since $\kappa = 12\pi^2 r \eta f_0$, where r is the radius of the particle. It is important to note that the fluid viscosity of water is highly temperature-dependent.²⁵ The absorption of a gold nanoshell changes with wavelength, and therefore the surface temperature of a nanoshell should also change with wavelength, affecting the local water viscosity. Additionally, the absorption of water changes with wavelength, affecting the temperature of the water within the trapping volume.

While several methods have been developed for determining the temperature in an optical trap, most of them require sophisticated optical setups or complex chemical systems.³⁴⁻³⁶ Here, we utilized a technique which required no additional equipment. The technique is based on approaches developed by Peterman *et al.*³⁷ and Abbondanzieri *et al.*³⁸ using the temperature-dependent viscosity in Eq. (2). At frequencies significantly higher than the corner frequency ($f \gg f_0$), the effect of corner frequency becomes negligible, and Eq. (1) becomes independent of trap stiffness. However, it remains dependent on the ratio of temperature to viscosity, which is a function of temperature when Eq. (2) is inserted for viscosity.²⁵ The effect of changing temperature can be seen from close inspection of the high-frequency region of the power spectra of a trapped particle as see in Figure 5. If the temperature were to remain constant as a function of wavelength, then the spectra should overlap at high frequencies. We see, however, that they do not overlap at different wavelengths, indicating a change in temperature as a function

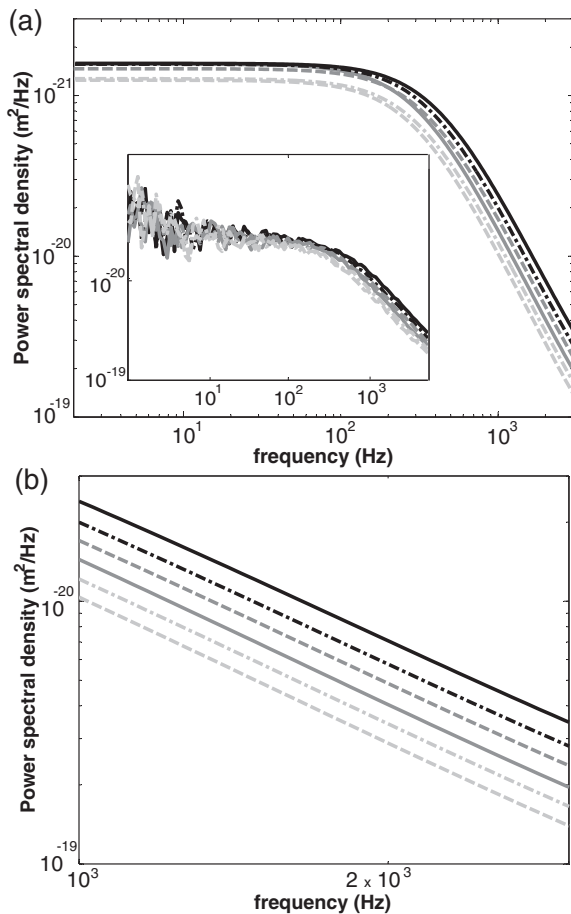


FIG. 5. (a) Lorentzian fits of power spectra for a single nanoshell trapped at several trapping wavelengths: Black solid line is 750 nm, black dash-dot line is 770 nm, dark grey dashed line is 790 nm, grey solid line is 810 nm, light grey dash-dot line is 830 nm, and light grey dashed line is 850 nm. Inset is the raw data corresponding to the fits. The optical power at the sample plane is maintained at 54 mW at each trapping wavelength. (b) High-frequency region of (a).

of wavelength. The temperature at each trapping wavelength was determined by analysis of the high-frequency region. The data was collected using a calibrated detector. Detector calibrations were performed at each trapping wavelength by moving a particle stuck to the coverslip through the center of the fixed Ti:sapphire laser beam.²⁸

We verified the accuracy of the temperature measurement by measuring the trap stiffness with two different methods. The power spectrum method, described above, utilized Eq. (1), where the trap stiffness is implicitly dependent on temperature. The second method used the equipartition of energy $\kappa = k_B T / \langle x^2 \rangle$, where x is the displacement of the particle from the trap center, and was only linearly dependent on temperature. A comparison of the two values for the trap stiffness determined with each method should not agree as a function of wavelength if the temperature is incorrect, and should closely agree if the correct values for temperature are used. As expected, the stiffnesses did not overlap when the temperature surrounding the nanoshell was assumed to be a constant at room temperature for each trapping wavelength (Figure 6(a)). When the measured temperature at each trapping wavelength was used, the trap wavelength dependence of the stiffnesses

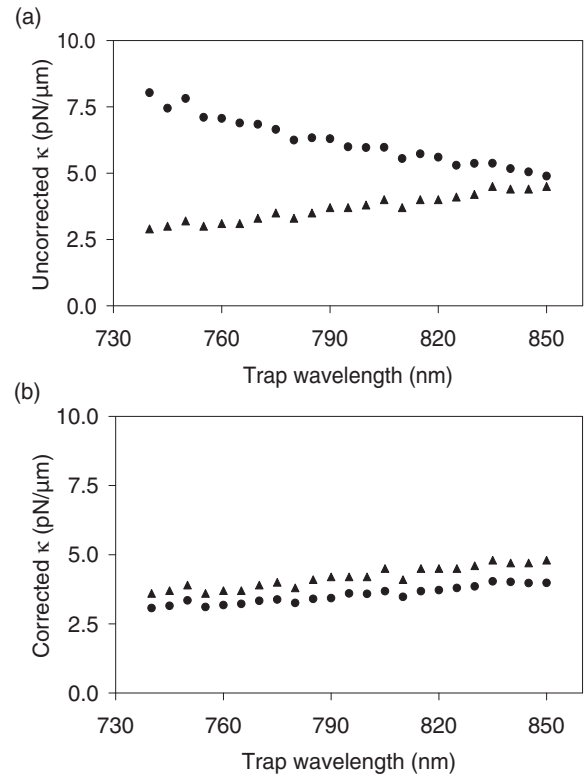


FIG. 6. Trap stiffness for the gold nanoshell described in Figures 2 and 3, measured over the trapping wavelength range. Circles are for data determined by the power spectrum method and triangles are for data determined by the equipartition method. (a) Stiffness with constant temperature assumed. (b) Stiffness with measured temperature incorporated into the stiffness determination.

agreed (Figure 6(b)). The agreement is not exact, however. The percent difference between the two stiffness values at each wavelength ranges from 0.2% to 7%, and is likely due in part to small errors in the detector calibration. Additionally, systematic differences are well-known and expected for results found by the equipartition and power spectrum methods. This is due to an underestimation of $\langle x^2 \rangle$ from finite sampling of x .³⁹ Since we are interested more in a change in temperature over our wavelength trapping range, and less in absolute values, we consider the close agreement of the stiffness in Figure 6(b) to be sufficient.

Clearly, changes in temperature (and therefore the viscosity) due to changing the trap wavelength in optical tweezers experiments for both absorbing and nonabsorbing particles trapped in water, must be included in system calibrations before accurate wavelength-dependent measurements can be realized. Other methods could be employed for determining temperature, including measurements with particles embedded in lipid membranes³⁵ and measurements of trapped particles subject to a well-known periodic motion of the sample chamber.³⁷ Viscosity could also be determined experimentally by utilizing a simultaneous analysis of CCD camera images of a trapped particle with position signals from a position detector.⁴⁰ It is important to note that repeating such measurements would be necessary for each trapping wavelength used in the data collection. Other experiments such as the measurement of trap stiffness versus ξ (the distance from coverslip to

trapped particle), trap stiffness versus laser power, and other measurements where temperature may be a changing experimental parameter may require a measurement of heating in order to obtain highly accurate results.

III. CONCLUSIONS

In the present work we have described a custom-built and versatile optical tweezer system with a set of experimental procedures allowing for the measurement of optical properties of single nano- or micro-particles as a function of wavelength. We avoided the more commonly used commercial inverted microscope in order to allow for a more adaptable system for studying different properties of a trapped particle. We currently measure the motion of a trapped particle with back focal plane interferometry, but the system could easily be altered to incorporate other light sources and detector types for a variety of measurements. With our apparatus, as long as the particle can be trapped, its optical properties (or perhaps other properties) may be studied. The properties of a material on a nano- or micro-scale sometimes differ from those for a bulk sample, and our apparatus may be utilized to examine these properties as the trapped particle size or optical trapping wavelength is changed. It may be possible that a laser with a broader wavelength range could be implemented into the system, allowing for more spectrally complete single particle measurements. In this case, more care should be taken to prevent changes in the trap size and changes in chromatic aberrations from affecting the experimental outcome.

An optical trap is a light-based system, therefore it is no surprise that changing the wavelength of the system will result in inherent changes in other properties. We have developed methods to prevent these changing properties from affecting the measurement outcomes, and have shown that these methods are able to isolate the wavelength dependence to the property being investigated. This was particularly important for the case of wavelength-dependent optical absorption where the temperature and viscosity of the trapped particle and surrounding fluid varied. Direct measurements of temperature were achieved in order to correct for this heating in measurements of the trap stiffness.

Future experiments that could be carried out with this apparatus include studies of index of refraction of particles, wavelength-dependent heating or other effects in biological systems, and wavelength-dependent effects in particles composed entirely of metal. In the future we plan to implement a more widely tunable laser and/or smaller particles to continue studies of trap stiffness and its relationship to optical extinction resonance. We expect this will lead to a deeper understanding of fundamental phenomena in optical trapping science.

ACKNOWLEDGMENTS

C.L.F., R.H., and N.J.H were supported by the Robert A. Welch Foundation (Grant Nos. C-1220 and C-1222), the Air Force Office of Scientific Research (Grant No. FA9550-10-1-0469), the Office of Naval Research (Grant No. N00014-10-1-0989), the DoD NSSEFF (Grant No. N00244-09-1-0067),

the Defense Threat Reduction Agency (DTRA) (Grant Nos. HDTRA1-11-1-0040), and the National Institutes of Health (Grant Nos. U01 CA 151886-01 and 5R01 CA151962-02). K.H. was supported by the Office of Naval Research (Grant No. N0001408IP20087). The authors thank Dr. Wolfgang Losert for fruitful discussions.

- ¹J. R. Moffitt, Y. R. Chemla, S. B. Smith, and C. Bustamante, *Annu. Rev. Biochem.* **77**, 205 (2008).
- ²K. Svoboda and S. M. Block, *Opt. Lett.* **19**, 930 (1994).
- ³C. Bustamante, J. C. Macosko, and G. H. L. Wuite, *Nat. Rev. Mol. Cell Biol.* **1**, 130 (2000).
- ⁴F. C. MacKintosh and C. F. Schmidt, *Curr. Opin. Colloid Interface Sci.* **4**, 300 (1999).
- ⁵P. L. Biancanello and J. C. Crocker, *Rev. Sci. Instrum.* **77**, 113702 (2006).
- ⁶K. Visscher, S. P. Gross, and S. M. Block, *IEEE J. Sel. Top. Quantum Electron.* **2**, 1066 (1996).
- ⁷K. Dholakia, W. M. Lee, L. Paterson, M. P. MacDonald, I. Andreev, P. Mthunzi, C. T. A. Brown, R. F. Marchington, and A. C. Riches, *IEEE J. Sel. Top. Quantum Electron.* **13**, 1646 (2007).
- ⁸K. Dholakia, M. P. MacDonald, P. Zemanek, and T. Cizmar, *Methods Cell Biol.* **82**, 467 (2007).
- ⁹M. M. Burns, J.-M. Fournier, and J. A. Golovchenko, *Phys. Rev. Lett.* **63**, 1233 (1989).
- ¹⁰A. Ashkin and J. M. Dziedzic, *Science* **235**, 1517 (1987).
- ¹¹W. C. K. Poon and D. Andelman, *Soft Condensed Matter Physics in Molecular and Cell Biology* (CRC, Boca Raton, 2006).
- ¹²Y. Liu, D. K. Cheng, G. J. Sonek, M. W. Berns, C. F. Chapman, and B. J. Tromberg, *Biophys. J.* **68**, 2137 (1995).
- ¹³M. Dao, C. T. Lim, and S. Suresh, *J. Mech. Phys. Solids* **51**, 2259 (2003).
- ¹⁴J. Ying, *Nanostructured Materials*, 1st ed. (Academic, San Diego, 2007).
- ¹⁵C. L. Nehl, N. K. Grady, G. P. Goodrich, F. Tam, N. J. Halas, and J. H. Hafner, *Nano Lett.* **4**, 2355 (2004).
- ¹⁶M. Nirmal, B. O. Dabbousi, M. G. Bawendi, J. J. Macklin, J. K. Trautman, T. D. Harris, and L. E. Brus, *Nature (London)* **383**, 802 (1996).
- ¹⁷J. M. Bingham, K. A. Willets, N. C. Shah, D. Q. Andrews, and R. P. Van Duyne, *J. Phys. Chem. C* **113**, 16839 (2009).
- ¹⁸A. B. Stilgoe, T. A. Nieminen, G. Knöner, N. R. Heckenberg, and H. Rubinsztein-Dunlop, *Opt. Express* **16**, 10539 (2008).
- ¹⁹R. R. Agayan, F. Gittes, R. Kopelman, and C. F. Schmidt, *Appl. Opt.* **41**, 2318 (2002).
- ²⁰A. Ashkin and J. M. Dziedzic, *Appl. Opt.* **20**, 1803 (1981).
- ²¹M. J. Kendrick, D. H. McIntyre, and O. Ostroverkhova, *J. Opt. Soc. Am. B* **26**, 2189 (2009).
- ²²N. Halas, *Opt. Photonics News* **13**, 26 (2002).
- ²³F. Gittes and C. F. Schmidt, *Methods Cell Biol.* **55**, 129 (1998).
- ²⁴K. Berg-Sørensen and H. Flyvbjerg, *Rev. Sci. Instrum.* **75**, 594 (2004).
- ²⁵M. Laliberté, *J. Chem. Eng. Data* **52**, 321 (2007).
- ²⁶K. Svoboda and S. M. Block, *Annu. Rev. Biophys. Biomol. Struct.* **23**, 247 (1994).
- ²⁷F. Gittes and C. F. Schmidt, *Opt. Lett.* **23**, 7 (1998).
- ²⁸K. C. Neuman and S. M. Block, *Rev. Sci. Instrum.* **75**, 2787 (2004).
- ²⁹L. Bosanac, T. Aabo, P. M. Bendix, and L. B. Oddershede, *Nano Lett.* **8**, 1486 (2008).
- ³⁰F. Hajizadeh and S. N. S. Reihani, *Opt. Express* **18**, 551 (2010).
- ³¹M. Li and J. Arlt, *Opt. Commun* **281**, 135 (2008).
- ³²M. J. Nasse and J. C. Woehl, *J. Opt. Soc. Am. A* **27**, 295 (2010).
- ³³S. N. S. Reihani and L. B. Oddershede, *Opt. Lett.* **32**, 1998 (2007).
- ³⁴H. Mao, J. R. Arias-Gonzales, S. B. Smith, I. Tinoco, Jr., and C. Bustamante, *Biophys. J.* **89**, 1308 (2005).
- ³⁵P. M. Bendix, S. N. S. Reihani, and L. B. Oddershede, *ACS Nano* **4**, 2256 (2010).
- ³⁶P. M. Celliers and J. Conia, *Appl. Opt.* **39**, 3396 (2000).
- ³⁷E. J. G. Peterman, F. Gittes, and C. F. Schmidt, *Biophys. J.* **84**, 1308 (2003).
- ³⁸E. A. Abbondanzieri, J. W. Shaevitz, and S. M. Block, *Biophys. J.* **89**, L61 (2005).
- ³⁹W. Wong and K. Halvorsen, *Opt. Express* **14**, 12517 (2006).
- ⁴⁰G. Pesce, A. Sasso, and S. Fusco, *Rev. Sci. Instrum.* **76**, 115105 (2005).
- ⁴¹Certain commercial equipment, instruments, or materials are identified in this paper to foster understanding. Such identification does not imply recommendation or endorsement by the National Institute of Standards and Technology, nor does it imply that the materials or equipment identified are necessarily the best available for the purpose.